Molecular Crystals and Liquid Crystals

Publication details, including instructions for authors and subscription information:
http://www.tandfonline.com/loi/gmcl20

Studies of Solidification Behavior and Molecular Interaction in Benzoic Acid-o-Chloro Benzoic Acid Eutectic System

S. S. Das [a], N. P. Singh [b], Tanvi Agrawal [b], Preeti Gupta [a], S. N. Tiwari [c] & N. B. Singh [a]

[a] Department of Chemistry, D. D. U. Gorakhpur University, Gorakhpur, India

[b] Department of Chemistry, U. P. Automous College, Varanasi, India

[c] Department of Physics, D. D. U. Gorakhpur University, Gorakhpur, India

Version of record first published: 18 Mar 2009

To cite this article: S. S. Das, N. P. Singh, Tanvi Agrawal, Preeti Gupta, S. N. Tiwari & N. B. Singh (2009): Studies of Solidification Behavior and Molecular Interaction in Benzoic Acid-o-Chloro Benzoic Acid Eutectic System, Molecular Crystals and Liquid Crystals, 501:1, 107-124

To link to this article: http://dx.doi.org/10.1080/15421400802697350

Mol. Cryst. Liq. Cryst., Vol. 501, pp. 107–124, 2009

ISSN: 1542-1406 print/1563-5287 online
DOI: 10.1080/15421400802697350

Taylor & Francis
Taylor & Francis Group

Studies of Solidification Behavior and Molecular Interaction in Benzoic Acid–o-Chloro Benzoic Acid Eutectic System

S. S. Das[1], N. P. Singh[2], Tanvi Agrawal[2], Preeti Gupta[1], S. N. Tiwari[3], and N. B. Singh[1]
[1]Department of Chemistry, D. D. U. Gorakhpur University, Gorakhpur, India
[2]Department of Chemistry, U. P. Automous College, Varanasi, India
[3]Department of Physics, D. D. U. Gorakhpur University, Gorakhpur, India

Phase diagram of benzoic acid (BA)–o-chloro benzoic acid (o-CBA) system has been studied by thaw melt method and the results show the formation of a simple eutectic mixture. Heats of fusion values of the components and eutectic mixture were determined with the help of differential scanning calorimeter. Excess Gibb's free energy (G^E), excess enthalpy (H^E), and excess entropy (S^E) of mixing of pre-, post-, and the eutectic mixture were calculated. FT-IR spectroscopic studies and ab initio calculations were done to have an idea about the nature of interaction between the molecules in the eutectic mixture. Linear velocities of crystallization of the two components and the eutectic mixture were determined at different undercoolings. Microstructural studies of BA and o-CBA showed the formation of broken lamellar and lamellar type microstructure, whereas for the eutectic mixture growth of flat crystals in different directions from a particular point was obtained. The isotropic as well as the anisotropic solidification behavior was studied. Jackson's roughness parameter was calculated. Modulus of ruptures of pure components and the eutectic mixture were determined. Results show that eutectics are nonideal mixtures, and some weak interactions are involved between the two components.

Keywords: computer simulation; crystallization; eutectic; flexural strength; microstructure; phase equilibrium

Address correspondence to S. S. Das, Department of Chemistry, D. D. U. Gorakhpur University, Gorakhpur 273001, India. E-mail: ssdas2002@rediffmail.com

INTRODUCTION

Studies on eutectic alloys are of potential interest in the field of metallurgy and material science [1]. The solidification of the liquid phase of the eutectic material is a complex process that depends upon the solidification dynamics and concentration phase separation. During recent years, studies on the solidification and microstructures of eutectic materials, especially organic eutectics, have been given greater attention by the researchers [2–9]. The organic eutectic systems can be used as model systems for predicting various properties of metallic alloys due to their low melting temperature. Beside this, eutectics and addition complexes are also analogues to metal eutectics and intermetallic compounds, respectively. Various physical properties such as solidification behavior, strength, thermal properties, and microstructures, etc. are very helpful in deciding the utility of these materials. The physical and chemical properties of the eutectics, molecular interaction, and other aspects can be well understood with the help of excess thermodynamic functions and computer simulation.

In the present article, we report a detailed investigation of phase diagram, solidification kinetics, microstructure and, Differential Scanning Calorimetry (DSC) studies on the BA–o-CBA system. The values of excess thermodynamic functions viz G^E, H^E, and S^E of pure components and the eutectic mixture were calculated with the help of their heats of fusion values obtained from DSC studies. Molecular interaction was studied with the help of Fourier Transform Infrared (FT-IR) spectroscopic studies and computer simulation. The microstructure of the pure components and the eutectic has been predicted on the basis of Jackson's roughness parameter (α) values. Modulus of ruptures of the eutectic and the pure components were also determined to compare the flexural strength of eutectic mixture with those of the pure components.

EXPERIMENTAL

Materials

BA (Ranbaxy) and o-CBA (S. D. Fine Chemicals) were purified by repeated crystallization from hot water. The melting points of purified BA and o-CBA were found to be $121.4^\circ C \pm 0.0^\circ C$ ($122.4^\circ C$) and $141.0^\circ C \pm 0.0^\circ C$ ($142.0^\circ C$), respectively. The literature values of the melting points are mentioned in the bracket.

Phase Diagram Studies

The phase diagram of BA–o-CBA system was studied by thaw melt method [10]. Appropriate amounts of BA and o-CBA were weighed

in glass tubes to prepare mixtures of different compositions. The glass tubes were sealed and then heated slightly above the melting temperatures of the components in an oil bath. The mixtures were homogenized by repeated melting, chilling, and crushing into fine powders. Thaw and true melting temperatures were determined with the help of a precision thermometer.

Undercooling

The undercooling temperature of different mixtures was determined by the method described elsewhere [10]. Accurate amounts of BA, o-CBA, and their mixtures of different mole fractions were taken in clean glass tubes, sealed, and immersed in an oil bath maintained at a temperature slightly above their melting points. The heating was stopped on complete melting, and the bath was allowed to cool at a slow rate. The difference between the true melting temperature and this temperature gives the value of the undercooling temperature.

Study of Kinetics of Solidification

The linear velocities of crystallization of BA, o-CBA, and their eutectic mixture were determined by the method described by Rastogi and Bassi [11]. The measurements were carried out in a U-shaped Pyrex glass tube (length 10.0 cm and diameter 0.8 cm) placed over a graduated scale. The tube was filled separately with fine powders of the components and the eutectic mixture and kept in an oil thermostat maintained at a temperature slightly above the melting temperature of the materials. The temperatures were maintained at different undercooling, and in each set of experiment performed separately a seed crystal of the material was introduced from one end of the U-tube. On the addition of the seed crystal, nucleation and crystallization started linearly in the tube. The time required for crystallization of the material for a definite length in the horizontal part of the tube was recorded. The linear velocity of solidification was then calculated.

Heat of Fusion Measurements

Values of heat of fusion of BA, o-CBA, and the eutectic mixture were determined from the DSC thermograms obtained with the help of differential scanning calorimeter (METTLER STAR SW 900) in a nitrogen atmosphere at a heating rate of 5°C/min.

FT-IR Spectral Studies

FT-IR spectra of the components and the eutectic mixture were recorded on a BRUKER spectrometer in the wavelength range 4000-2000 cm^{-1} using KBr pellets.

Computational Studies

The optimized geometries of BA and o-CBA molecules were obtained by using an ab initio (GAMESS) program [12]. The net charge and dipole components located at each of the atomic centres of these molecules have been computed using GAMESS program fitted with 6-31G* basic set. The intermolecular interactions between the molecules were evaluated using second order perturbation theory modified by Calliet and Claverie for short intermediate range interaction.

Microstructural Studies

Small amount of fine powders of BA, o-CBA, and the eutectic mixture were placed on separate glass slides. These slides were kept in an oven maintained at a temperature slightly above their melting temperatures. The melts were crystallized by moving separate glass cover slips over them in one direction. The photographs of the crystallized front of the microstructures were recorded with the help of a digital camera attached to an optical microscope (Olympus CH i 20) at a magnification of 50 X and 100 X. Microstructures of the eutectic in the presence of 1.0 wt% α-naphthol and p-toluidine were also recorded. Apart from the anisotropic growth, the isotropic growth of the materials was also studied. For studying the isotropic growth, small amounts of the materials were kept on the glass slides and melted in an oven. These slides were kept immediately over ice cubes, and the crystallizations were allowed to occur by moving glass coverslips over them in one direction. Due care was taken in keeping the slides over the ice and moving the glass coverslips simultaneously.

Measurement of Modulus of Rupture

The samples were melted in a uniform cylindrical glass tube and then dropped vertically into an ice bath maintained at $\sim 0^{\circ}C$. After complete solidification of the sample, the glass tube was slowly scrapped off to give solid cylindrical shaped samples. These cylindrical samples were placed on the stand as shown in Fig. 1. A small container was hung in the middle of the cylindrical sample with the help of a metallic wire.

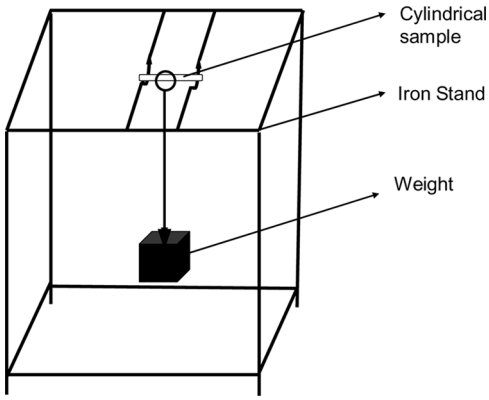

FIGURE 1 Apparatus for determination of flexural strength.

Known weights were then placed in the container until the cylindrical sample got ruptured. Modulus of rupture σ_{fs} of the materials was calculated with the help of Eq. (1) [13]:

$$\sigma_{fs} = \frac{F_f L}{\pi R^3}, \tag{1}$$

where F_f is the load at fracture, L is the distance between support points, and R is the specimen radius.

RESULTS AND DISCUSSION

The temperature composition curve of BA–o-CBA system as obtained by phase diagram studies is shown in Fig. 2. From the phase diagram, it is clear that a simple eutectic is formed at 0.3292 mole fraction of o-CBA melting at $95.0^{\circ}\mathrm{C} \pm 0.0^{\circ}\mathrm{C}$. The undercooling curve is also shown in Fig. 2.

The linear velocities of crystallization (v) for BA, o-CBA, and the eutectic mixture at different undercooling (ΔT) are shown in Fig. 3. The linear velocity of crystallization is related to the undercooling (ΔT) by Hillig Turnbull [14] Eq. (2):

$$\mathrm{v} = \mathrm{k}(\Delta\mathrm{T})^{\mathrm{n}}, \tag{2}$$

where k is kinetic coefficient and n is a constant; k and n are known as crystallization parameters and depend on the solidification behavior of the materials. The values of k and n are determined from the

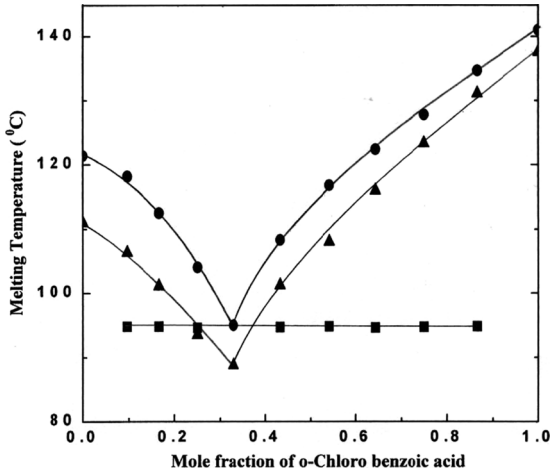

FIGURE 2 Phase diagram of BA–o-CBA system; (●) melting temperature, (■) Thaw melting temperature, (▲) undercooling temperature.

intercept and the slope of the straight lines obtained by plotting log v against log ΔT (Fig. 3). The experimental values of k and n are given in Table 1.

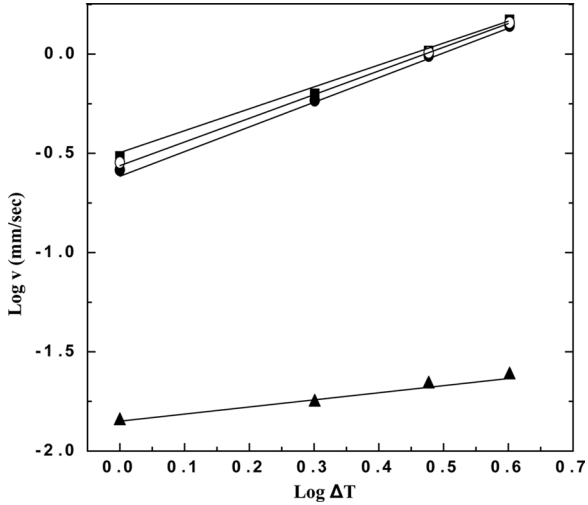

FIGURE 3 Linear velocities of crystallization at various undercoolings; (■) BA, (●) o-CBA, (▲) Eutectic (Experimental), (○) Eutectic (mixture law).

TABLE 1 Crystallization Parameters and Heats of Fusion for BA, o-CBA, and the Eutectic Mixture

System	k (mm s^{-1})	n (mm $s^{-1}{}^{\circ}C^{-1}$)	Heat of fusion (Jg^{-1})
Benzoic acid	0.3021 ± 0.0070	1.12 ± 0.06	152.70
o-Chlorobenzoic acid	0.2630 ± 0.0000	1.19 ± 0.02	175.86
Eutectic (experimental)	0.0143 ± 0.0002	0.36 ± 0.01	137.44
Eutectic (mixture law)	0.2818 ± 0.0000	1.15 ± 0.04	160.32

The linear velocity of crystallization (v) for the eutectic system was also calculated with the help of mixture law (Eq. (3))

$$v = x_1 v_1 + x_2 v_2, \tag{3}$$

where x_1 and x_2 are mole fractions of components 1 and 2, and v_1 and v_2 are the linear velocities of components 1 and 2, respectively. The log v values obtained from the mixture law were plotted against log ΔT (Fig. 3) which also gave a straight line. It is clear from Fig. 3 that at different undercoolings, the linear velocities of crystallization for the eutectic mixture, calculated with the help of mixture law, are higher than the experimental values. This suggests the possibility of some type of molecular association or weak interaction between BA and o-CBA. The eutectic system cannot be considered as a mechanical mixture of the two pure components [15]. The results of linear velocities of crystallization (Table 1) suggest that the value for the eutectic is less than the values for the pure components BA and o-CBA. This clearly indicates that solidification mechanism follows alternate nucleation of the two components [16].

The nature of interaction between the two components forming a eutectic can be known by obtaining heats of fusion values of the pure components and the eutectic mixture. The experimental heat of fusion values were determined from DSC measurements, while the calculated values of heat of fusion as obtained from the mixture law (Eq. (4)) are given in Table 1:

$$(\Delta H_f)_e = (x_1)_e(\Delta H_f)_1 + (x_2)_e(\Delta H_f)_2, \tag{4}$$

where $(\Delta H_f)_1$ and $(\Delta H_f)_2$ are the heats of fusion of components 1 and 2, respectively. On comparing the two values, it is observed that the experimental heat of fusion value of the eutectic mixture is lower than the calculated heat of fusion value. This suggests that some kind of interaction between the two components exists in the eutectic mixture. Further, the results show that the heat of fusion values of BA and

o-CBA are higher than those of the eutectic mixture. This could be explained due to a lower magnitude of interaction between the two components in the eutectic mixture in comparison to those present in the individual components viz BA and o-CBA.

An attempt has been made to calculate the total interaction energy $(H_m^1 + \sigma_{L^-S}A + \epsilon)$ with the help of Eq. (5):

$$(\Delta H_f)_e = [(\Delta H_f)_e]_{\text{mix law}} + H_m^1 + \sigma_{L^-S}\, A + \epsilon, \tag{5}$$

where

$$\epsilon = [(\Delta H_f)_e]_{exp} - [(\Delta H_f)_e]_{cal}$$

and

$$[(\Delta H_f)_e]_{cal} = (x_1)_e(\Delta H_f)_1 + (x_2)_e(\Delta H_f)_2.$$

The total interaction energy thus calculated from Eq. (5) is found to be 3.05 kJ/mol.

The FT-IR spectra of BA, o-CBA, and their eutectic mixture are shown in Fig. 4. The results of the spectral studies have revealed that BA has a dimeric structure due to a strong intermolecular hydrogen bond. The stretching vibration of H-bonded OH group appears at

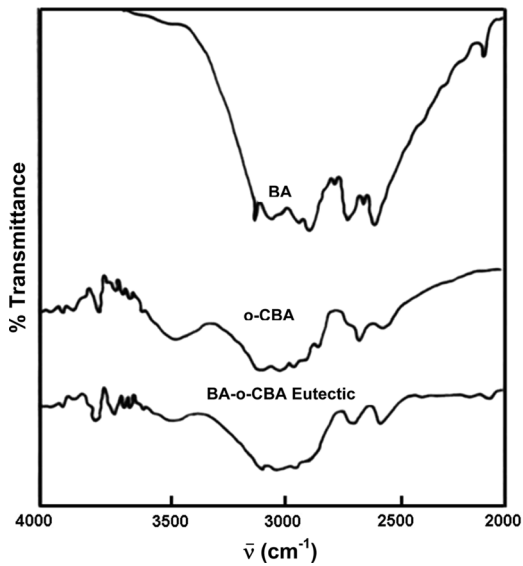

FIGURE 4 FT-IR spectra of BA, o-CBA and the eutectic mixture.

3071.8 cm^{-1}, which is much lower than the stretching frequency of free OH, generally observed at ~3600 cm^{-1}. In case of o-CBA, a broad band appearing at 3447.8 cm^{-1} indicates H-bonded OH group in the acid. However, in the case of the BA–o-CBA eutectic mixture a broad band of low intensity appears at 3455.1 cm^{-1}. This indicates that during the formation of eutectic mixture, the dimeric structure of BA is broken, and a weak H-bond is formed between BA and o-CBA giving an organized geometry to the eutectic mixture.

Further, considering the molecular structure there is a possibility of dipole–dipole interaction as well as weak charge transfer interaction between the two component molecules in the eutectic mixture. These results clearly indicate the presence of weak molecular interaction between the components in the eutectic mixture.

The optimized molecular geometries of BA and o-CBA are shown in Fig. 5. The net charge and dipole components corresponding to each atomic center of the BA and o-CBA molecules are given in Tables 2 and 3, respectively. As expected, oxygen atoms (O_8 and O_9) associated with the acid group (-COOH) possess maximum electronegative charges, while the carbon atom (C_7) of the same group bears highest electropositive charge amongst all the atoms of the BA molecule (Table 2). Net charge on various atoms in o-CBA molecule has been slightly modified (Table 3). This is likely because of the introduction of chlorine atom at the ortho position in the BA molecule. All hydrogen atoms bear electropositive charges. Like hydrogen atoms, the chlorine atom also carries electropositive charge, although very small (0.07236 e.u.). Due to the introduction of chlorine atom, asymmetry of the molecule is increased. This point is strengthened as the value of dipole moment of o-CBA is higher than that of the BA molecule.

Intermolecular interactions between BA and o-CBA molecules have been evaluated during stacking and in-plane (side-by-side) configurations [17]. During stacking interactions, one of the molecules is kept fixed while in the other molecule both positional as well as angular variations were simultaneously introduced and vice versa. The variation of total stacking energy with interplanar separation has been shown in Fig. 6. As evident from this figure, a sharp and deep minimum is obtained at 3.4 Å with energy of -11.8 $kcalmol^{-1}$. To obtain the minimum energy configuration, further calculations were carried out with accuracies 0.1 Å in translation and 1.0 Å in rotation. The final optimum energy stacked configuration thus obtained, (depicted in Fig. 7a) bears an energy of -12.32 $kcalmol^{-1}$ at an interplanar separation of 3.1 Å between BA and o-CBA. The in-plane (side-by-side) interactions have also been evaluated by placing both the molecules in one

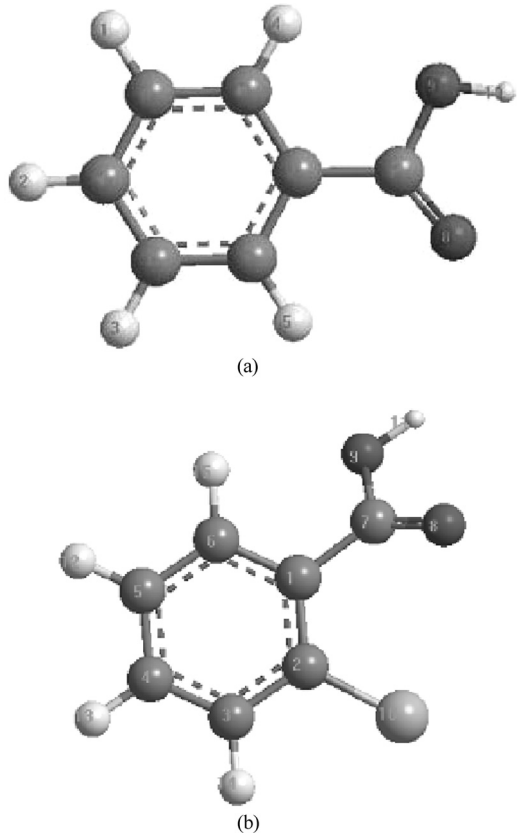

FIGURE 5 (a) Optimized geometry of Benzoic acid; (b) Optimized geometry of o-CBA.

plane and introducing lateral and angular variations in one of the interacting molecules with respect to the other molecule keeping fixed and vice versa. The minimum energy configuration of BA and o-CBA during side-by-side interaction is shown in Fig. 7b. The optimum distance between the centers of mass positions of the interacting molecules is 6.8 Å with energy $-32.36\,\text{kcal}\,\text{mol}^{-1}$. The energy during in-plane interactions is higher (by nearly two times) than that of the stacking interaction energy, which indicates a strong possibility of hydrogen bond formation between the molecules. These results clearly indicate that in the eutectic mixture, there is a weak electrostatic interaction, possibly H-bond between BA and o-CBA. Because of this, the eutectic mixture has a stable configuration.

TABLE 2 Molecular Charge Distribution in BA as Calculated by GAMESS Program Using 6-31 G* Basis Set

Atom number	Atomic Symbol	Charge (e.u.)	Dipole component (Debye)		
			X	Y	Z
1	C	−0.14756	−0.01392	0.02052	0
2	C	−0.16488	0.06532	−0.11814	0.00702
3	C	−0.21887	−0.08937	−0.08960	−0.00781
4	C	−0.17403	−0.09182	0.00484	0.00879
5	C	−0.21794	−0.05629	0.09976	0.01580
6	C	−0.16964	0.01979	0.07566	−0.00253
7	C	−0.81307	0.07770	0.05595	0.00702
8	O	−0.60942	−0.87256	1.21352	0.00309
9	O	−0.74067	0.89193	−1.27147	−0.00261
10	H	0.25702	−0.10732	0.12055	−0.00167
11	H	0.21418	0.07276	0.14253	0
12	H	0.21618	0.16090	0.01007	−0.00281
13	H	0.21313	0.08297	−0.14684	0
14	H	0.25438	−0.12179	−0.12210	0
15	H	0.47505	−0.07894	0.08600	0.00310
Total	Dipole	Moment		2.74 D	

TABLE 3 Molecular Charge Distribution in o-CBA as Calculated by GAMESS Program Using 6–31 G* Basis Set

Atom number	Atomic Symbol	Charge (e.u.)	Dipole component (Debye)		
			X	Y	Z
1	C	−0.06262	0.01656	0.03130	−0.02780
2	C	−0.12669	0.04331	0.07162	0.00377
3	C	−0.19829	0.08638	−0.11448	0
4	C	−0.17166	0.12077	−0.03579	−0.00544
5	C	−0.21687	0.02854	0.09054	−0.01435
6	C	−0.16618	−0.07630	0.07825	−0.01269
7	C	0.75442	−0.08558	0.07531	−0.00360
8	O	−0.57282	0.96904	0.89770	0.70258
9	O	−0.72282	−1.04888	−0.90636	−0.75492
10	Cl	0.07236	1.08966	1.97470	−0.18959
11	H	0.23735	−0.03776	0.16761	−0.00523
12	H	0.22425	−0.16339	0.00253	−0.00254
13	H	0.21965	−0.08510	−0.13110	0.00925
14	H	0.25473	0.09756	−0.12817	−0.00300
15	H	0.47518	0.08732	0.03838	0.02040
Total	Dipole	Moment		3.79 D	

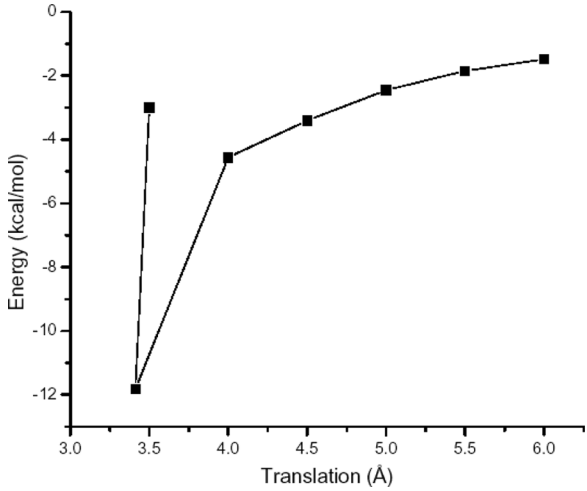

FIGURE 6 Potential energy diagram with respect to translation for the interaction of a pair of BA and o-CBA molecules.

Due to weak molecular interactions, BA and o-CBA molecules align in a definite way in the eutectic mixture. The deviation from ideal behavior can be expressed with the help of excess thermodynamic functions. The values of excess thermodynamic functions are also very important in the quantitative analysis of the nature of molecular interactions [15]. Thus in order to have an idea about the nature of interaction between two components forming the eutectic, some excess thermodynamic functions such as excess Gibb's free energy (G^E), excess enthalpy (H^E), and excess entropy (S^E) were determined in a manner similar to that reported earlier [15,18] from the solidus–liquidus equilibrium data of BA–o-CBA system which obeys the phase equilibrium relation.

The calculated values of G^E, H^E, and S^E are given in Table 4. The variations of G^E, H^E, and S^E with the mole fraction of o-CBA are shown in Fig. 8. The minimum values of G^E at the eutectic composition thus indicate maximum stability of the eutectic mixture. The negative values of H^E and S^E in the entire composition range of the BA–o-CBA system indicates the non ideal nature of the system.

Various physical properties of the eutectic materials depend on their microstructures. Therefore, the microstructures (Figs. 9 and 10) of BA, o-CBA, and the eutectic can explain their crystallization behavior more easily. BA and o-CBA when crystallized anisotropically show broken lamellar and lamellar type microstructures (Figs. 9a, b), respectively, with a very little spacing between the two lamellae. On the other hand, in the case of eutectic, the microstructure (Fig. 9c) is

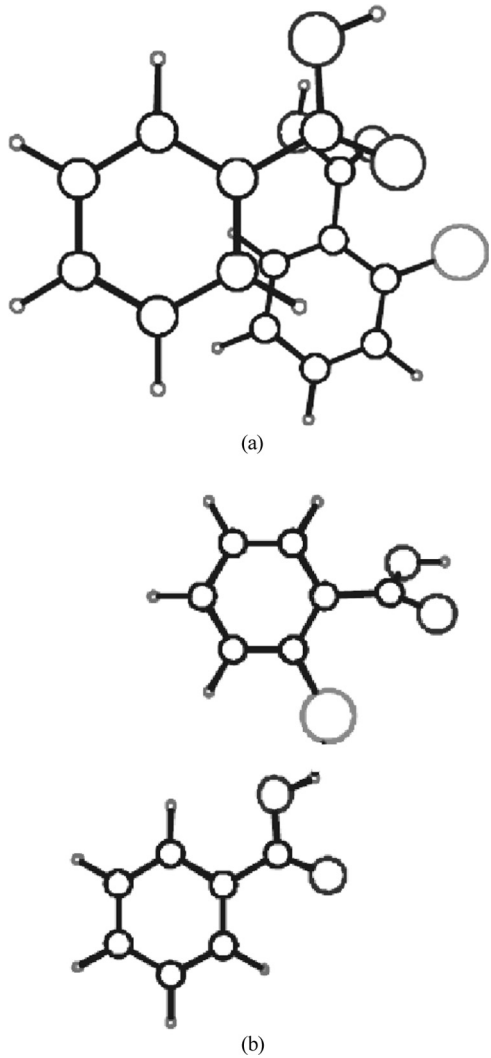

FIGURE 7 (a) Minimum energy configuration of BA and o-CBA during stacking interactions with interplanar distance 3.1 Å and energy $-12.32\,\text{kcalmol}^{-1}$; (b) Minimum energy configuration of BA and o-CBA during side-by-side interactions. The optimum distance between the center of mass positions of the two molecules is 6.8 Å with energy $-32.36\,\text{kcalmol}^{-1}$.

completely different. In this growth of flat crystals in different directions from a particular point is clearly noticed. In the presence of 1% p-toluidine as an impurity in the eutectic, the anisotropic

TABLE 4 Activity Coefficient ($\ln\gamma_1$, $\ln\gamma_2$), Excess Gibbs Free Energy (G^E), Excess Enthalpy (H^E), and Excess Entropy (S^E) of BA–o-CBA Eutectic System

Mole fraction of o-CBA (x_1)	Mole fraction of BA (x_2)	$\ln\gamma_1$	$\ln\gamma_2$	$\frac{\partial \ln\gamma_1}{\partial T}$	$\frac{\partial \ln\gamma_2}{\partial T}$	G^E (kJ mol^{-1})	H^E (kJ mol^{-1})	S^E (J mol^{-1}K^{-1})
0.0976	0.9024	1.8606	0.0562	0.0186	0.0143	0.755	−18.734	−49.821
0.1667	0.8333	1.2002	0.0512	0.0203	0.0147	0.778	−19.342	−52.193
0.2500	0.7500	0.6012	0.0255	0.0221	0.0154	0.531	−20.146	−54.846
0.3292	0.6708	0.1111	−0.0083	0.0235	0.0161	0.095	−20.885	−57.013
0.4325	0.5675	0.1521	0.3713	0.0221	0.0149	0.877	−21.755	−59.355
0.5417	0.4583	0.1164	0.7073	0.0212	0.0141	1.254	−22.695	−61.443
0.6429	0.3571	0.0655	1.0441	0.0207	0.0135	1.364	−23.573	−63.069
0.7536	0.2464	0.0194	1.4915	0.0202	0.0127	1.273	−24.538	−64.401
0.8657	0.1343	0.0206	2.1916	0.0196	0.0112	1.058	−25.508	−65.161

microstructure (Fig. 9d) appears in the form of thin needle shaped crystals. However, in the case of 1% 1-naphthol as an impurity in the eutectic the microstructure (Fig. 9e) shows the formation of rectangular intermingled crystals.

The microstructures obtained after isotropic crystallization are entirely different from the anisotropic ones. The isotropic microstructure of BA (Fig. 10a) appears like a bundle of bamboos. The isotropic

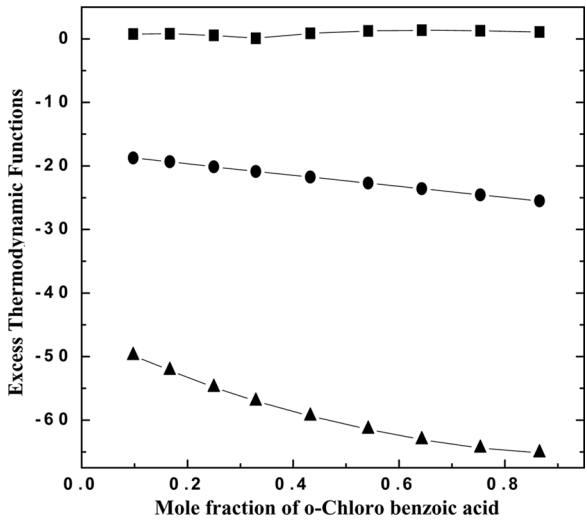

FIGURE 8 Excess thermodynamic functions of BA–o-CBA system; (■) excess Gibbs energy (GE), (●) excess Enthalpy (HE), (▲) excess Entropy (SE).

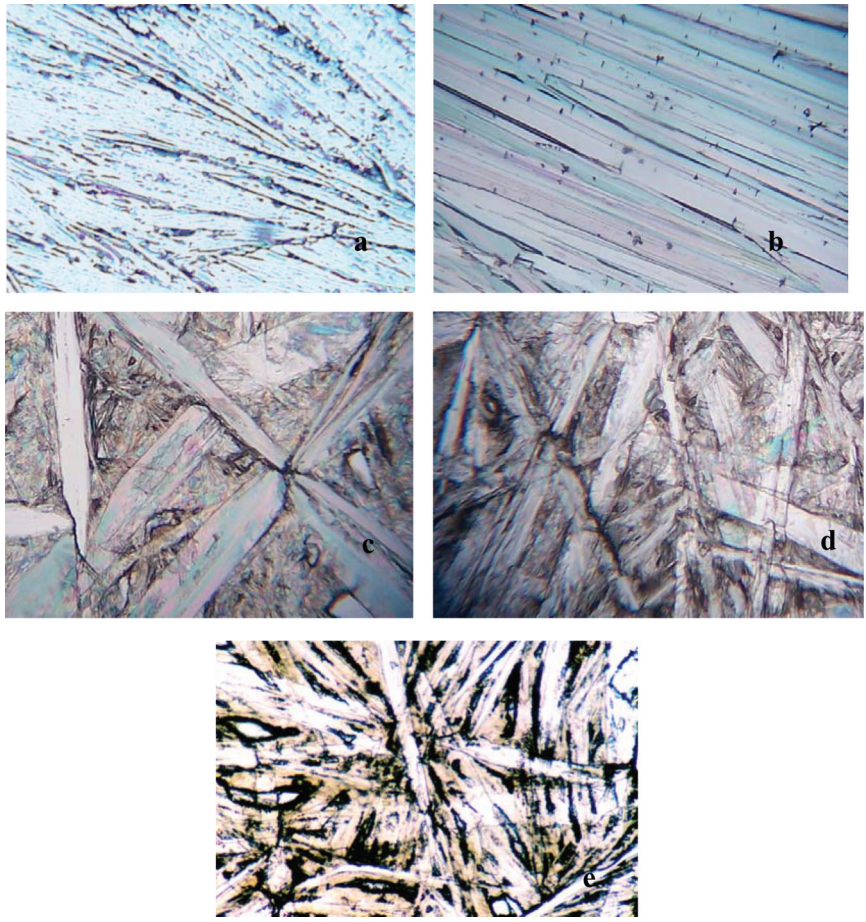

FIGURE 9 Anisotropic microstructures at 100 X magnification: (a) BA, (b) o-CBA, (c) Eutectic, (d) Eutectic with 1% p-toluidine, and (e) Eutectic with 1% 1-naphthol.

microstructure of o-CBA (Fig. 10b) shows the formation of bamboos of small diameters growing in different directions. The isotropic microstructure of the BA–o-CBA eutectic is entirely different from those of the components. In this case formation of small crystallites can be seen (Fig. 10c). In case of isotropic growths when the same impurities viz 1-naphthol and p-toluidine were added in the eutectic the microstructures (Figs. 10d, e) showed the formation of star like patterns in which crystallization seems to occur from one point in different directions. It has been reported [4] that the formation of microstructures

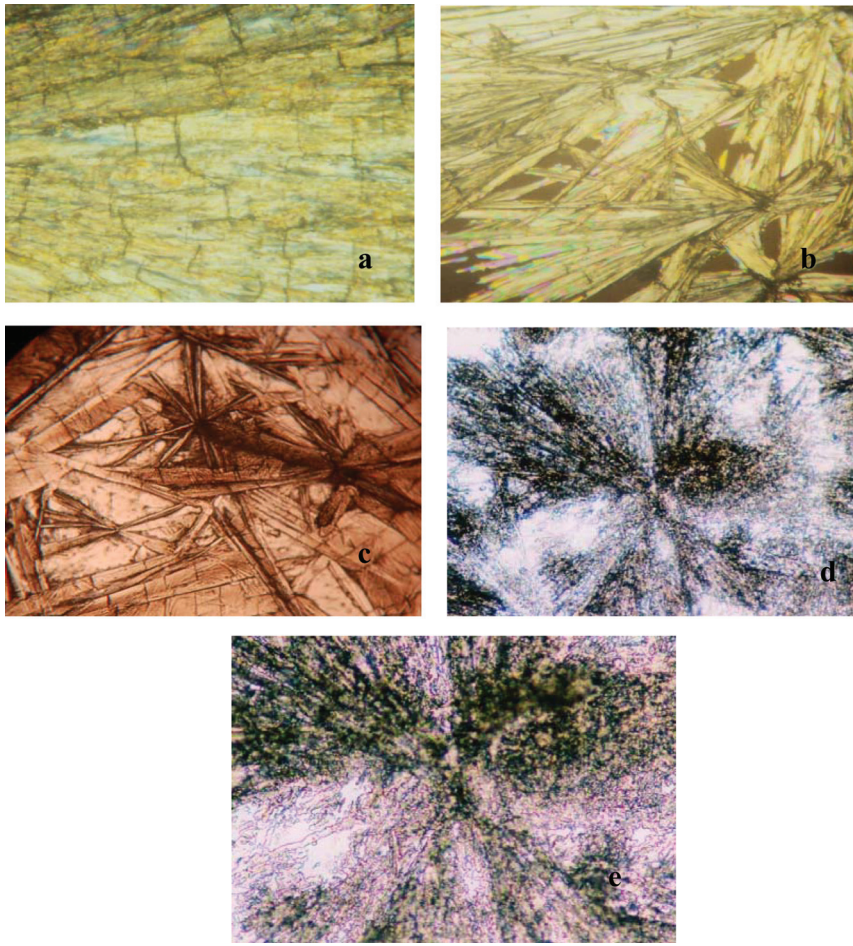

FIGURE 10 Isotropic microstructures at 100 X magnification: (a) BA, (b) o-CBA, (c) Eutectic, (d) Eutectic with 1% p-toluidine, and (e) Eutectic with 1%1-naphthol (except Fig. 10d at 50 X magnification).

depend on various factors such as the nature and molecular structure of the components, concentration gradient, interface contact angles, diffusion, nucleation and crystallization characteristics of the two phases, chemical inhomogenities and types of defects present in the growing nuclei. Since it is very difficult to know these parameters precisely, therefore it is not possible to predict the microstructure of the eutectic correctly. However, Hunt and Jackson [19] were able to predict the structure of the solid/liquid interface in terms of roughness parameter

TABLE 5 Values of Jackson's Roughness Parameter for BA, o-CBA, and the Eutectic Mixture

System	Jackson's roughness parameter ($\xi = 0.5$) $Jmol^{-1}$	Jackson's roughness parameter ($\xi = 1.0$) $Jmol^{-1}$
Benzoic acid	9.2	13.8
o-CBA	11.7	17.6
BA–o-CBA eutectic	3.0	6.0

(α) of the eutectic system with the help of Eq. (6):

$$\alpha = \xi \frac{\Delta H_f}{RT}, \tag{6}$$

where ξ is the geometrical coefficient whose value lies between 0.5–1.0, ΔH_f is the heat of fusion, T is the temperature and R the gas constant. The values of α for the two components and the eutectic mixture were calculated by putting ξ value equal to 0.5 and 1.0, respectively. The two α values thus obtained are given in Table 5. Both the values of α for the eutectic are greater than 2. It is reported that for the values $\alpha > 2$, the solid/liquid interface is atomically smooth and the crystal develops a faceted morphology with an irregular structure. It is reported [19] that the faceted morphology will never give a regular structure. Thus it may be inferred that the present BA–o-CBA eutectic mixture ($\alpha > 2$) is expected to possess faceted morphology with an irregular structure.

The results on modulus of rupture show that the flexural strength of the components is practically negligible. This may be due to breaking of the cylindrical sample during isotropic growth. On the other hand, the flexural strength of the eutectic material was found to be 2.03 ± 0.04 Mpa which is much higher than those of the components. This may be due to alignment of the components in the eutectic mixture in a definite fashion leading to higher flexural strength.

CONCLUSION

Phase diagram studies have revealed the formation of simple eutectic mixture. Heat of fusion data calculated from mixture law, excess thermodynamic functions, and linear velocity of solidification data show that eutectic is a nonideal mixture. FT-IR spectroscopic studies have indicated the possibility of weak hydrogen bond between the two

molecules in the eutectic mixture. Stacking interaction energy in the eutectic mixture, determined from ab initio calculations, also showed the possibility of strong hydrogen bonding between the two molecules. The microstructure of the eutectic is changed in the presence of 1-naphthol and p-toluidine. Isotropic and anisotropic growths revealed different microstructures. It is also found that flexural strength of the eutectic is much higher than those of the components.

REFERENCES

[1] Elliott, R. (1983). *Eutectic Solidification Processing*, Butterworths: London.
[2] Chalmers, B. (1964). *Principles of Solidification*, John Wiley & Sons: New York.
[3] Elder, K. R., Gunton, J. D., & Grant, M. (1996). *Physical Review*, E, *54*, 6476.
[4] Singh, N. B., Das, S. S., Singh, N. P., & Agrawal, T. (2008). *J. Crys. Growth*, *310*, 2878.
[5] Gupta, R. K., Singh, S. K., & Singh, R. A. (2007). *J. Crys. Growth*, *300*, 415.
[6] Witusiewicz, V. T., Hecht, U., Sturz, L., & Rex, S. (2006). *J. Crystal Growth*, *286*, 431.
[7] Gupta, R. K., & Singh, R. A. (2004). *J. Crys. Growth*, *267*, 340.
[8] Singh, N. B., Giri, D. P., & Singh, N. P. (1999). *J. Chem. Eng. Data*, *44*, 605.
[9] Rai, U. S. (1994). *J. Crys. Growth*, *144*, 291.
[10] Rastogi, R. P., & Verma, K. T. R. (1956). *J. Chem. Soc.*, 2097–2101.
[11] Rastogi, R. P., & Bassi, P. S. (1964). *J. Phys. Chem.*, *68*, 2398.
[12] Levine, I. N. (2006). *Quantum Chemistry* (5th Ed.), Pearson Prentice Hall: New Delhi, 551.
[13] Callister, W. D., Jr. (2005). *Materials Science and Engineering: An Introduction* (6th Ed.), John Wiley & Sons, Inc.: New York, 412.
[14] Hillig, H. B., & Turnbull, D. (1956). *J. Chem. Phys.*, *24*, 914.
[15] Sharma, B. L., Kant, R., Sharma, R., & Tondon, S. (2003). *Mater. Chem. Phys.*, *82*, 216.
[16] Wingard, W. C., Majka, S., Thall, B. M., & Chalmers, B. (1954). *Can. J. Chem.*, *29*, 320.
[17] Claverie, P. (1978). *Intermolecular Interactions: From Diatomics to Biopolymers*, Pullman, B. (Ed.), John Wiley & Sons, Inc.: New York.
[18] Singh, N. B., Das, S. S., Gupta, P., & Dwivedi, M. K. (2008). *J. Cryst. Growth. 311*, 118.
[19] Hunt, J. D., & Jackson, K. A. (1966). *Trans. Metall. Soc. AIME*, *236*, 1129.